Szilard's Engine as a Quantum Thermodynamical System

Maryam Ashrafi,[1,*] Kyle J. Ray,[1,†] Fabio Anza,[2,1,‡] and James P. Crutchfield[1,§]

[1] *Complexity Sciences Center and Physics Department, University of California at Davis, One Shields Avenue, Davis, CA 95616*

[2] *InQubator for Quantum Simulation (IQuS), Department of Physics, University of Washington, Seattle, WA 98195, USA*

(Dated: December 5, 2022)

We analyze an engine whose working fluid consists of a single quantum particle, paralleling Szilard's construction of a classical single-particle engine. Following his resolution of Maxwell's Second Law paradox using the latter, which turned on physically instantiating the demon (control subsystem), the quantum engine's design mirrors the classically-chaotic Szilard Map that operates a thermodynamic cycle of measurement, thermal-energy extraction, and memory reset. Focusing on the thermodynamic costs to observe and control the particle and comparing these in the quantum and classical limits, we detail the thermodynamic tradeoffs behind Landauer's Principle for information-processing-induced thermodynamic dissipation in the quantum and classical regimes. In particular, and as found with the classical engine, we show that the sum of the thermodynamic costs over a cycle obeys a generalized Landauer Principle, exactly balancing energy extraction from the heat bath. Thus, the quantum engine obeys the Second Law. However, the quantum engine does so via substantially different mechanisms: classically measurement and erasure determine the thermodynamics, while in the quantum implementation the cost of partition insertion is key.

Keywords: Landauer Principle, heat engine, information engine, Maxwell Demon, quantum thermodynamics

I. INTRODUCTION

Sparked by Maxwell's thought experiment on the limitations of the Second Law [1], modern efforts to improve our understanding of nanoscale processes have clearly highlighted information as a thermodynamic resource [2–4]. Starting with Szilard's insights [5], then going through later work by Landauer [6], Bennett [7], and many others [8], the modern developments of stochastic [9] and information [10] thermodynamics allow us to appreciate Maxwell's demon as an *information engine* [11, 12]—a physical system whose dynamical evolution simultaneously stores and processes information in the service of a desired cycle of thermodynamic transformations.

While originally formulated in the classical domain, the inherent microscopic character of these analyses, together with dramatic improvements in our ability to manipulate systems at the nanoscale, invites us to re-examine these engines to account for quantum behavior. In fact, quantum Maxwell demons and Szilard engines have been widely discussed [13–29] and experimentally realized [30–36]. The following takes a complementary approach with respect to existing explorations, though, as it builds on the mechanistically-detailed version of Szilard's engine introduced in Refs. [11, 37].

While a fully accurate description of engine operation requires accounting for the underlying dynamics, we focus on two crucial aspects of a quantum Szilard engine. First, recognizing the physical role of the information processing exerted by the control subsystem, we give a microscopically-detailed treatment of this so-called demon by giving it physical form. Second, we improve on the description of the costs arising in each of the distinct stages of the engine's thermodynamic cycle—measurement, thermal-energy extraction, and reset. This involves analyzing how each stage's operation depends on the physical parameters at play.

To do so, we parallel the dynamical-systems analysis performed in Ref. [11] that highlighted the interplay between the entropic cost of erasure and measurement, and how they depend on both system and demon parameters. The result is a plethora of thermodynamic phenomena in which entropic costs of measurement, erasure, and control are traded-off against each other, while still respecting Landauer's Principle [38].

In particular, unlike the classical engine, the quantum version incurs a cost when inserting a partition divider. The upshot is that the quantum engine, too, obeys the Second Law, via a generalized Landauer's Principle, though due to different mechanisms. This achieves a more detailed exploration of the engine as a *thermodynamical system*—a dynamical system whose evolution of microstate distribu-

* ma.ashrafi91@gmail.com
† kjray@ucdavis.edu
‡ fanza@uw.edu
§ chaos@ucdavis.edu

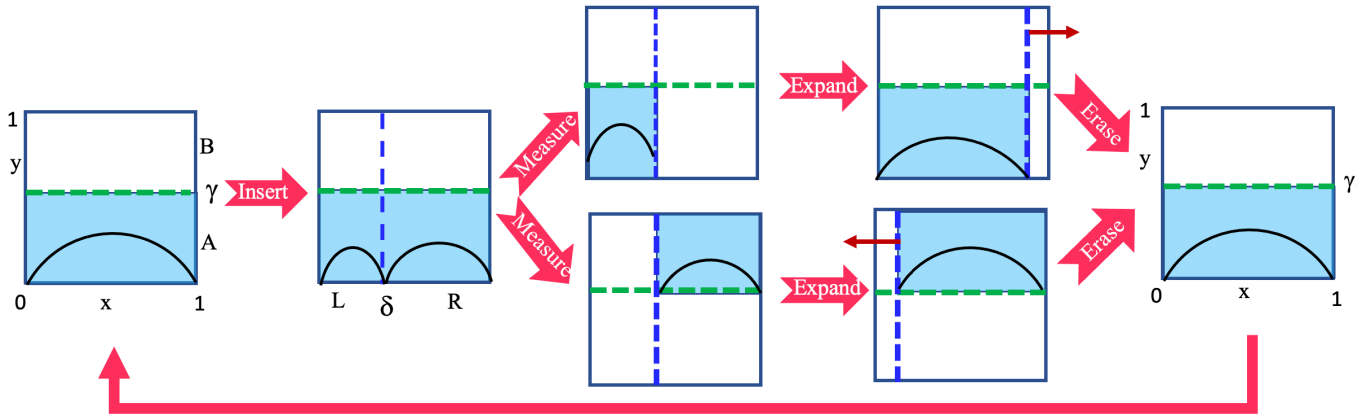

FIG. 1. Quantum Szilard engine thermodynamic cycle: Insert partition, measure particle location, expand, and erase memory of particle location to reset joint system state to begin next cycle. Cf. actions of the classical engine under control of the Szilard Map in Ref. [11]'s Fig. 1. The horizontal dimension (x) is the state of the quantum particle. The vertical dimension (y) is the state of the demon (control) subsystem. δ determines the location of the partition upon insertion (vertical dashed blue line). γ delineates the boundary of the demon's two memory states (horizontal dashed green line). The solid blue curve is a schematic representation of the quantum particle's wavefunction. The light blue shaded region tracks the region of positive probability for the joint (particle,demon) state.

tions supports macroscopic thermodynamic transformations.

Our aim is to go beyond Landauer's Principle, though, to uncover the dynamical interplay between thermodynamic costs, dynamic evolution, and (quantum) information processing. This provides a comprehensive picture. The thermodynamic costs are analyzed in detail in classical and quantum regimes. Then, before drawing conclusions, we briefly review related results on alternative quantum Szilard engines.

II. ENGINE DESIGN

The *Quantum Szilard Engine* (QSE) is an ideal system with which to examine the role of information processing during thermodynamic transformations. The engine consists of two components: the *system under study* (SUS), and a quantum controller or *demon*. Together, they are surrounded by an incoherent *environment* that maintains the composite system in thermal equilibrium at inverse temperature β.

As noted above, a wide diversity of physical instantiations have been proposed. Here, following the classical engine introduced by Ref. [11], we model the joint system as a single quantum particle in a 2D box of square geometry, with sides of unit length. Horizontal and vertical axes, $x, y \in [0, 1]$, represent the continuous degrees of freedom of SUS and demon, respectively. Figure 1 lays out the individual transformation the comprise the engine's cyclic operation.

Paralleling the classical engine's thermodynamic cycle, the QSE steps through a repeating sequence of four functionally-distinct operations or stages: *insertion*, *measurement*, *control*, and *erasure*. Each of these stages is implemented by changing the potential energy surface according to a deterministic protocol.

In the first stage of the engine's cycle a potential barrier is inserted at $x = \delta$. Then, a coarse-grained projective measurement is performed on the SUS position, correlating whether it is left (L) or right (R) of the barrier with the state of the demon. To track the measurement outcome two relevant informational demon states A and B are identified: A with the box's lower area $y \leq \gamma$ and B with the upper area $y > \gamma$. γ controls measurement fidelity—how much particle positional information is stored in the demon's memory states.

The result is that the joint state space (unit square) is partitioned in four macrostates: $\{AL, BL, AR, BR\}$, where $\{L \sim x \in (0, \delta], R \sim x \in (\delta, 1)\}$ and $\{A \sim y \in (0, \gamma], B \sim y \in (\gamma, 1)\}$. The projector onto a given macrostate's subspace can be directly written as:

$$\Pi_{AL} = \int_L dx \int_A dy \, |x, y\rangle \langle x, y|$$

and similarly for Π_{AR}, Π_{BL}, and Π_{BR}. Subscripts denote informational mesostates.

Without loss of generality, we take the demon's reference (initial) state to be A. Thus, if the particle is found in macrostate L, the demon need not update its memory state; it does nothing. If the particle is found in position mesostate R, though, the demon updates its memory state

to mesostate B. The informational mesostates of the joint system resulting from this action is described by a CNOT gate [39], correlating the left-right measurement outcome with the demon's upper-lower informational mesostate:

$$A \otimes L \to A \otimes L$$
$$A \otimes R \to B \otimes R \ .$$

Then, the barrier is released and allowed to move (right or left) contingent on the demon memory state (A or B), respectively. In this way, energy is extracted from the heat bath by the support of the wave-function expanding to fill the whole volume. Finally, the composite system is reset to its original state A to prepare the engine for a new cycle. Figure 1 also shows the joint system's informational states.

There are two relevant features to call out. First, the SUS and demon operate as a joint quantum system. Second, δ controls the barrier's location and so the SUS mesostate. Similarly, γ controls how the position mesostate maps into the demon informational mesostates. With this setup, the thermodynamic analysis can explore the interplay between the resource costs and information processing during the cycle stages as a function of δ and γ, respectively.

The following first recalls the thermodynamics of a particle in a 1D box in the semi-classical and quantum regimes. It then describes the quantum thermodynamics at each engine stage. Details of the numerical evaluations and analytical calculations will appear elsewhere.

III. THERMODYNAMICS OF A PARTICLE IN A BOX

To put the analysis in context, it is helpful to first review the core aspects of the thermodynamics of a quantum particle in a 1D box of length ℓ. Its energy levels are:

$$E_n = \frac{n^2 \pi^2 \hbar^2}{2m\ell^2} \ , \qquad n \in \mathbb{N}_+ \ .$$

The partition function:

$$Z = \sum_n e^{-\beta E_n}$$

can be written in terms of the Jacobi function:

$$Z = \frac{1}{2}\left(\theta_3(0,q) - 1\right) \ ,$$

where:

$$\theta_3(0,q) = \sum_{i=-\infty}^{\infty} q^{i^2} \ ,$$

with:

$$q \equiv \exp\left[-\pi \left(\lambda_{\rm d}/2\ell\right)^2\right] \ .$$

Here, $\lambda_{\rm d}(T) = \sqrt{2\pi\hbar^2/mk_{\rm B}T}$ is the thermal de Broglie wavelength, and $-\ln q = \beta E_1$ is the measure of coldness in the ground state energy scale. The relevant features that determine the operating regimes are (i) the size of the box ℓ, to be compared with $\lambda_{\rm d}$, and (ii) the boundary conditions, given using the standard Dirichlet prescription of zero value at the boundary and outside the box.

Conveniently, the wavelength $\lambda_{\rm d}$ (directly) and parameter q (implicitly) determine the system's degree of quantumness. This then identifies the physical regimes:

- Classical—$\lambda_{\rm d} \ll \ell$ with partition function:

$$Z^{\rm C} = \tfrac{1}{2}\sqrt{\pi/|\ln q|} \ .$$

- Quantum—$\lambda_{\rm d} > \ell$ where we must use the exact form:

$$Z^{\rm Q} = \left(\theta_3(0,q) - 1\right)/2 \ .$$

As all thermodynamic quantities are computed via derivatives of the partition function, a quantitative analysis that holds across all temperature needs an accurate evaluation of the partition function and its low-degree derivatives at any temperature.

To this end, we compare the classical approximations against a high-precision numerical evaluation of the full partition function. The crucial difference with the exact case is given by the change in $Z(T)$'s convexity at low temperatures, which is not reproduced by the classical approximation. Since Z's convexity, determined by the behavior of second-order derivatives, governs fluctuations, the classical approximation predicts dramatically different thermal fluctuations at low temperatures. Thus, even though the system consists of a single particle, and so lacks phase-transition-like phenomena (e.g., Bose-Einstein condensation), a fully quantum expression is still needed to appropriately model macroscopically relevant quantities, together with their fluctuations, at low temperatures.

Below a temperature T_1 with $k_B T_1 = E_2 - E_1$—i.e., $\lambda_{\rm d} \gg \ell$ ($q < .2$)—the system is effectively in its ground state, with a nonvanishing energy given by the zero point and a vanishing von Neumann entropy. This means that energy and entropy fluctuations are actively suppressed below a certain temperature.

Assuming that at the end of each engine stage the particle subsystem is in a Gibbs' canonical state, the internal

energy is:

$$\begin{aligned} U &= \mathrm{Tr}\, H\rho \\ &= -\partial \log Z/\partial\beta \end{aligned}$$

and the entropy is:

$$\begin{aligned} S &= -k_{\mathrm{B}}\, \mathrm{Tr}\, \rho \log \rho \\ &= k_{\mathrm{B}} \left(1 - \beta \tfrac{\partial}{\partial\beta}\right) \ln Z \ , \end{aligned}$$

where ρ is the density matrix.

Using this framework, a sequel reports detailed expressions for the thermodynamic bookkeeping of entropy, internal energy, and work, as a function of the parameters δ and γ in three physical regimes: classical, ground state, and quantum. It compares the thermodynamic costs when only the ground state is populated, as is usually done for very low temperature with the exact full quantum regime, illustrating how increasing temperature populates additional energy levels. The results highlight the appreciable differences between the ground-state populated temperature dependencies and the exact quantum dependencies that account for higher-energy eigenstates. From this, one appreciates how both the barrier position δ and the memory partition γ directly affect thermodynamic costs of insertion. Below, we highlight and discuss certain results from this analysis. The appendix contains these results in a simplified form.

IV. INITIALIZATION

The QSE is prepared in a reference state in which the demon (controller subsystem) is in a thermal state localized to the lower part of the box—demon mesostate A—while the SUS is in a thermal state with full support on $x \in [0, 1]$. Let $\rho_{x,y}(\delta, \gamma)$ be a generic Gibbs' canonical state of the joint system and $Z_{x,y}(\delta, \gamma)$ its partition function, where the dependence on the previously defined parameters δ and γ is made explicit. Accordingly, we call $\rho_x(\delta)$ and $\rho_y(\gamma)$ the Gibbs' canonical state of SUS and demon, respectively, and $Z_x(\delta)$ and $Z_y(\gamma)$ their respective partition functions. With these definitions, the initial configuration of the engine is $\rho_x(1) \otimes \rho_y(\gamma)$ with partition function $Z_x(1)Z_y(\gamma)$ and energy levels $E_{\mathrm{SUS}} + E_{\mathrm{demon}}$.

V. INSERTION

Keeping in mind the classical engine's operation, we now show that the most distinctive step in the quantum engine cycle arises from the partition's isothermal insertion. To model insertion we follow Refs. [40, 41]'s treatment: the barrier is described by a very thin δ-function potential $V(t) = \lambda(t)\delta(x-\delta)$. As $\lambda(t) \to \infty$, barrier insertion erases all coherence between the particle residing on either side. This occurs for all energy eigenstates, thus the same loss of coherence holds for canonical states.

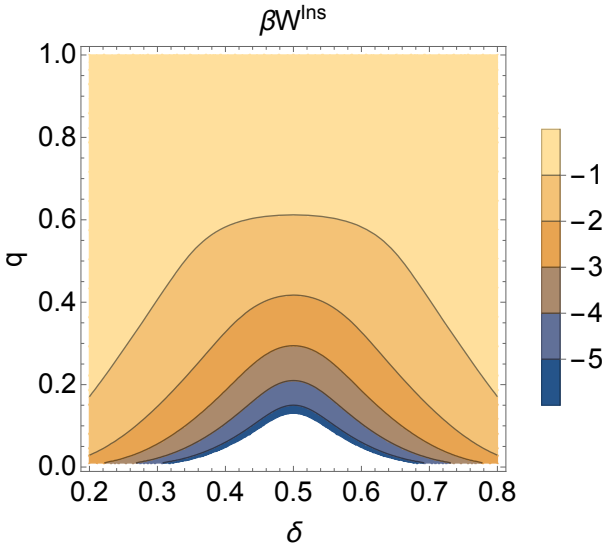

FIG. 2. Thermodynamic work cost W^{ins} of inserting the partition at locations $\delta \in [0, 1]$ as a function of temperature for $\hbar = 1$ and $2m = \pi^2$. The legend at right gives the values of βW^{ins}. The thermodynamic work cost maximizes at $\delta = 1/2$. With increasing temperature the insertion work decreases, vanishing in the classical limit.

This is a key observation that arises from a dynamical argument regarding the partition's physical nature. So, the suppression of the off-diagonal matrix elements occurs due to the barrier's insertion, not the projective measurement of particle position. This step substantially modifies the thermodynamic cost of measurement, while leaving unaltered the sum of its own cost and the measurement's. We note that, based on a completely different argument, Ref. [14] also draws this same conclusion.

Accordingly, the energy cost due to destroying coherences does not occur due to measurement, but instead due to insertion. This thermodynamics differs markedly from the classical case in which insertion has no cost. That said, the transformation renders the engine's density matrix an incoherent superposition between left and right positions *before measurement*. In this way, the classical limit recovers the classical result of no thermodynamic cost for insertion.

Figure 2 shows the dependence of insertion work as a function of partition parameter $\delta \in [0, 1]$. At low temperature the insertion cost is very sensitive to the place of insertion and is maximum at $\delta = 1/2$. Increasing the temperature, the work cost of the insertion and its dependence on δ

decreases as the classical case is smoothly recovered.

VI. MEASUREMENT AS INDUCED CORRELATION

In the quantum domain, the practical aspects of measurement are nontrivial. And so, a more detailed development is necessary than for the classical engine. The second (measurement) stage of the quantum engine's cycle comes in two steps. First, it implements a coarse-grained projective measurement of the SUS. Then, it implements a CNOT gate that correlates the measurement result (L or R) with the demon mesostate (A or B).

If the particle is found on the left, the demon does nothing, as it was already initialized to the A mesostate. Otherwise, it changes mesostate from A to B. Therefore, the measurement cost contains two parts. The first is a localization cost that is symmetric about δ. The second is the cost of storing the information in the demon's memory. It is not symmetric in δ. The asymmetry arises from the CNOT gate, which is not symmetric with respect to L and R.

Appropriate thermodynamic bookkeeping reveals the average changes in internal energy, entropy, and work. The values are computed averaging over the probability distribution $(p_L(\delta), p_R(1-\delta))$ of finding the particle on the barrier's left or right side after insertion, where $p_L(\delta) = Z_x(\delta)/\left(Z_x(\delta) + Z_x(1-\delta)\right)$ and $p_R(1-\delta) = 1 - p_L(\delta)$.

Figure 3 displays p_L, the probability of being in the left compartment after insertion. Classically, the probability should just be δ, the size of the partition. In the case that the system stays in its ground state through the insertion, the particle is found with probability 1 to be in the larger compartment, so $p_L = 0$. Between these two extremes lies an interesting regime with nontrivial behavior where the probabilities depart from the classical case very rapidly when $q < 1$ unless $\delta = .5$. Due to this, a full quantum treatment is necessary for large swaths of the parameter space.

Moreover, the protocol's specific properties affect the thermodynamic bookkeeping in a nontrivial way. For example, symmetric barrier insertion ($\delta = 1/2$) leads to an insensitivity to quantum effects. Sensitivity is regained, though, for even small changes: e.g., $\delta = 12/25$. The existence of this and other nontrivial interplay between system parameters and the temperature highlights the need for detailed analysis of this stage.

For example, Fig. 3 demonstrates that using the classical approximation has a qualitative impact on thermodynamic accounting as the functional dependence on the system parameters, such as temperature, are strongly affected by quantum effects except in special cases.

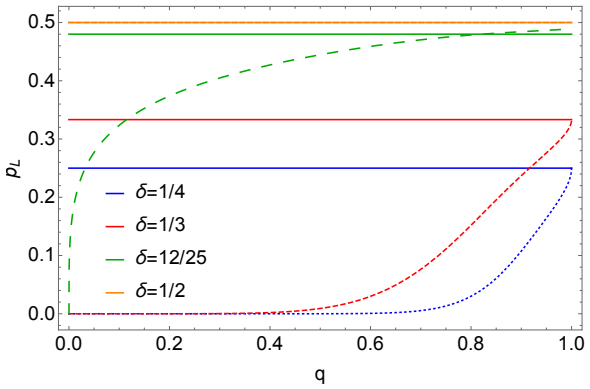

FIG. 3. Temperature dependence of the probability of finding the particle on the left side at various insertion positions $\delta \in \{1/4, 1/3, 12/25, 1/2\}$. Dashed lines give the quantum probability and solid lines, classical. The validity of the classical assumption, and the ground state assumption are clearly affected by the interplay between the system's parameter δ and the temperature.

To this end, Fig. 4 shows how the heat and work depend on both the partition insertion parameter δ and demon memory parameter γ; see App. A. Considering both the demon and its quantum nature allows probing beyond $\gamma = 0.5$ to account, for example, for experimental uncertainties. This markedly changes the thermodynamics of measurement, resulting in nonzero contributions for both the energetic and work cost. Furthermore, one can appreciate how the symmetry $\delta \leftrightarrow 1-\delta$—that one naively expects to hold—is present if and only if the demon informational mesostates are truly equivalent, as it does not hold unless $\gamma = 0.5$.

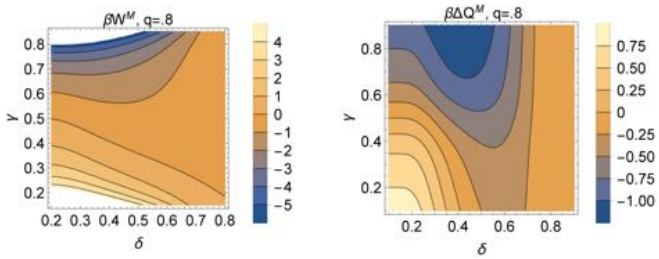

FIG. 4. Partition location δ and demon memory γ dependence of thermodynamic heat $\beta\Delta Q_{\mathrm{M}}$ and thermodynamic work $\beta\Delta W_{\mathrm{M}}$ during measurement and correlation steps as a function of δ and γ at $q = 0.8$. Due to asymmetry in the initial memory state the measurement cost is not symmetric respect to δ.

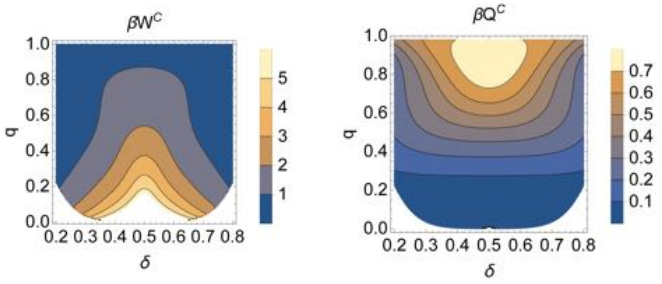

FIG. 5. Thermodynamic work cost βW^{C} and heat transfer $\beta Q^{\mathrm{C}}$of expansion at locations $\delta \in [0,1]$ as a function of q. For $\delta = 1/2$ the maximum work is extracted from the system. In the very low temperature limit, the heat transfer vanishes and the work done by the system equals the change of the particle's internal energy. At high temperatures, the internal energy change vanishes and the work done on the system equals the heat transfer.

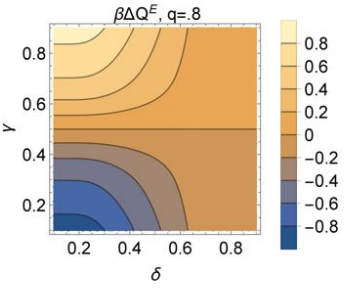

FIG. 6. Dissipated heat $\beta\Delta Q_E$ during erasure at $q = 0.53$. Nonmonotonic behavior of $\beta\Delta Q_E$ in $|\delta - 0.5|$ results from the lack of symmetry between the informational mesostates at $\gamma \neq 1/2$.

VII. CONTROL

After measurement and contingent on the appropriate mesostate, the partition moves isothermally to the left (right), thereby extracting $W^C = -\sum_n P_n dE_n$ of work from the ambient heat bath. In short, the control stage's thermodynamic costs are independent of the details of the demon's informational mesostates, while still exhibiting dependence on temperature and partition parameter δ. Figure 5 reveals several interesting results. While both the extracted work and the entropic cost monotonically decrease as $|\delta - 0.5|$ increases, the internal energy change depends only on the temperature and not on δ. (See App. A for the details.)

VIII. ERASURE

The engine's last stage returns the joint particle-demon system to its original configuration, preparing the engine to begin a new thermodynamic cycle. Landauer originally claimed that all thermodynamic cost arose from the erasure stage and not measurement [38]. Much later, it was shown that this was far too restrictive [11]: depending on partition insertion and demon memory mesostates, work and heat costs can be traded-off. As we now show, this holds in the quantum engine, except via notably different mechanisms.

Figure 6 reveals interesting nonmonotonic behavior in the dissipated heat as a function of δ and γ. Here, we note that at $\gamma = 0.5$, where the demon's informational mesostates are symmetric, there is no work or energy cost associated with the erasure. Again, this is explained in terms broken $\delta \leftrightarrow 1 - \delta$ symmetry—a symmetry present only on the line $\gamma = 0.5$. While reasonable in certain cases, this neglects structural imperfections and experimental uncertainties or even intentionally designed differences between the demons memory states.

Figure 7 confirms this by showing that the erasure work cost vanishes only when the demon informational states have such symmetry—viz., $\gamma = 1 - \gamma = 1/2$. If $\gamma \neq 1/2$, there is a nonzero work-cost to account for, whose value depends on both γ and δ.

Meanwhile, Fig. 8 displays how quickly the ground state can be reached when $\gamma = \delta$. Even for values of q as high as 0.5 or 0.6, the erasure costs can be neglected as the system settles into its (deterministic) ground state where $p_L = 0$.

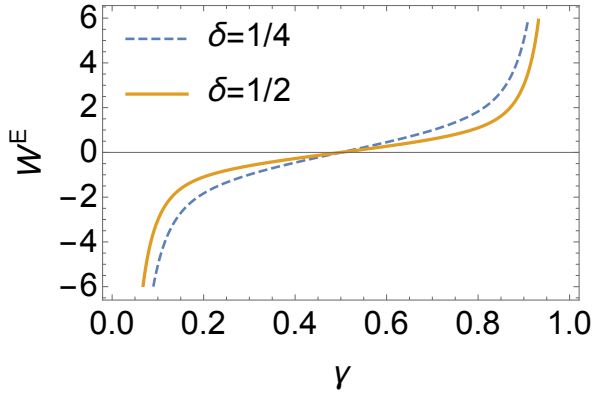

FIG. 7. Erasure work W^{E} as a function of demon mesostate A size (γ) for $q = 0.95$. The erasure work cost vanishes only for the symmetric case $\gamma = 1/2$, even in the near-classical regime.

IX. DISCUSSION

This development extends the recent dynamical analysis [11] of Szilard's classical single-particle engine. It modeled the Szilard engine as a quantum information engine consisting of a simple quantum system interacting with

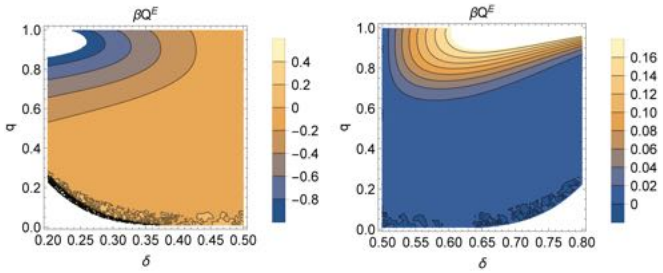

FIG. 8. $\beta\Delta Q_{\mathrm{E}}$ during measurement and correlation steps as a function of $\delta{=}\gamma$ and q. The erasure cost vanishes for $\delta < .5$. This points towards the demon and SUS both being in the ground state.

a control system—the demon. Taking to heart Szilard's original strategy to solve Maxwell's paradox, we analyzed the physics of both the thermodynamic system and control system. Agreeing with Szilard, over the entire thermodynamic cycle the net changes—resource uptake or exhaust—balance each other out. There is zero output work and the operation is consistent with the Second Law:

$$\Delta U^I + \Delta U^C = 0$$
$$\Delta U^M + \Delta U^E = 0 \ ,$$

and:

$$\Delta Q^I + \Delta Q^C = -(\Delta Q^M + \Delta Q^E) \ ,$$
$$W^I + W^C = -(W^M + W^E) \ .$$

That said, portions of the quantum engine's cycle exhibit novel behavior and new trade-offs. In particular, they show a nontrivial relationship to Landauer's Principle. Specifically, the aggregate entropic cost of measurement and erasure still satisfies it (see App. A):

$$\langle Q_{erase} \rangle + \langle Q_{measure} \rangle = \beta^{-1} \ln 2 H(\delta) \ ,$$

where $H(\delta)$ is the binary entropy function. References [42–45] previously noted this for the classical engine.

While the Second Law is not violated—all entropic contributions sum to zero, see Fig. 9—the thermodynamic signature of the individual stages varies significantly. Thus, these thermodynamic trade-offs are key to designing quantum engines.

For example, at $\delta = \gamma = 1/2$, the entropic cost of erasure vanishes, "violating" Landauer's Principle. However, it still respects the trade-off thanks to the fact that $\langle Q_{measure} \rangle = \log 2$. The bottom panel of Fig. 9 illustrates the change of the thermodynamic costs $\Delta Q/k_{\mathrm{B}}T$ from very low to very high temperatures. In the ground state regime measurement cost and erasure cost vanish and the insertion cost equals in magnitude the control cost.

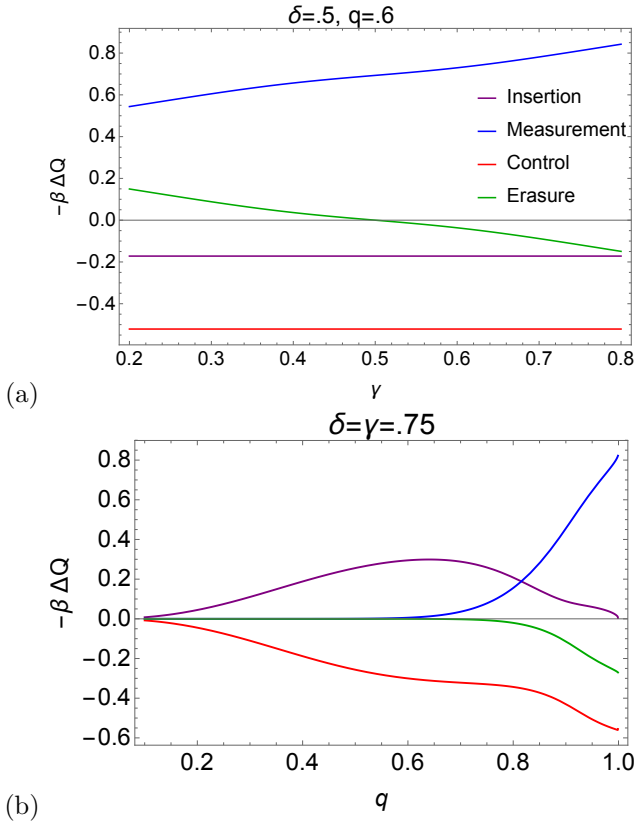

FIG. 9. Thermodynamic costs $\beta\Delta Q$ versus demon memory-mesostate parameter γ for measurement (blue dash line), control (red dotted line), and erasure (green solid line). The sum of measurement and erasure costs equals the sum of insertion and control work. (a) For $q = .6$ and $\delta = 1/2$. The cost of erasure is zero for $\gamma = 1/2$. (b) Thermodynamic costs $\Delta Q/k_{\mathrm{B}}T$ versus q for $\delta = \gamma = .75$. In the low temperature limit, the cost of the measurement and erasure vanish, while at high temperature the cost of insertion vanishes. Note that once in the ground state limit—here, approximately $q < .5$—the cost of measurement and erasure vanishes and the cost of insertion equals the expansion cost.

Looking at the other end of the spectrum: in the very high temperature limit, insertion cost vanishes and the sum of the erasure and control costs equal (in magnitude) the measurement cost.

X. RELATED WORK

As the introduction noted, quantum Szilard engines have been widely analyzed [13–29, 46] and experimentally implemented [30–36], forming an interesting set of results that collectively aim to clarify the physical role of information processing in nanoscale systems and its interplay with the energetics.

That said, the specific motivating questions, implementations, and interpretations differ widely across these works.

Here, we briefly mention several with the goal of providing a bird's eye view and highlighting the advantages of the dynamical-maps approach we pursued here. We begin surveying theoretical results.

Zurek and Lloyd's work [47, 48] was the first of the modern wave of contributions leveraging tools from quantum information theory and quantum thermodynamics. See also the more recent reviews of Refs. [14, 16, 17, 19, 29]. Interestingly, Refs. [27, 49] highlight differences between single and multi-particle Szilard engines. While Refs. [18, 50–52] show how, despite equilibrium assumptions, the thermodynamic costs of each stage of the quantum engine can qualitatively depend on details of the quantum model, while recovering the classical results in the high temperature limit.

Over the last decade or so, there also has been a number of experimental investigations reported under the rubric of quantum Maxwell demons and Szilard engines. In this, one finds an even wider variation on what constitutes physically implementing demons.

To the best of our knowledge, Ref. [30] was the first experimental implementation of a quantum Szilard engine that extracts $k_{\mathrm{B}}T\ln 2$ of work per one bit of information. Analogously, Ref. [33] realized an NMR-based quantum Szilard engine, while Ref. [35] implemented a direct "information to work" conversion with a superconducting (transmon) platform. Maxwell demons have also been implemented on a photonic platform [34] and on solid-state spin systems [32].

Overall, there is agreement that these constructions are consistent with the Second Law, once the appropriate role of information processing is recognized. However, stage-specific thermodynamic costs can depend on model details, complicating a universal understanding of the interplay between energetics and information processing.

This diversity motivated our parametrized analysis—an exploration that accounts for model details via the parameters δ and γ. The analysis also addressed the difference in behaviors in the classical and quantum regimes. Moreover, reflected on this background, our analysis differs in that it starts with a quantum counterpart of constructions in Ref. [11, 37] that explicitly implement each of Szilard's transformations. In effect, each step in the engine's thermodynamic cycle is a piecewise linear map on the macrostates of the joint system, with an associated quantum transformation—essentially a particle in a 2D box with time-varying boundaries. This led to detailed thermodynamic bookkeeping for each engine stage, with quantitative results that track parameter dependence. Modeling the engine stages with dynamical maps provided a direct connection to quantum dynamical systems. The latter's perspective is often not included in quantum thermodynamics of nanoscale systems. For that matter, the conclusion from the classical analysis—that the physics and information dynamics are both essential—holds with extra force in the quantum domain.

XI. CONCLUSION

We revisited Szilard's engine from the broader perspective of a quantum information engine—a quantum machine that manipulates both energy and information to produce work while dissipating heat. Including both the parametric dependence on the informational states of the demon, and its quantum nature, into the engine's description allowed us to explore a variety of nonclassical thermodynamic behaviors. Those behaviors, while compatible with the principles of quantum thermodynamics, exhibited new and different thermodynamic signatures. We believe these analyses generalize to arbitrary quantum information engines and will be an aid in designing efficient quantum information processing devices.

ACKNOWLEDGMENTS

F.A. and J.P.C. thank the Telluride Science Research Center for its hospitality during visits and the participants of its annual Information Engines summer workshop for stimulating discussions. This material is based on work supported by, or in part by, a Templeton World Charity Foundation Power of Information Fellowship, Foundational Questions Institute Grant FQXi-RFP-IPW-1902, and U.S. Army Research Laboratory and the U. S. Army Research Office grants W911NF-18-1-0028 and W911NF-21-1-0048.

Appendix A

The following summarizes the analytical results derived in a sequel, used for both plotting and discussion.

Before Insertion:

$$
\begin{aligned}
Z^{(0)} &= Z_x(1)Z_y^A(\gamma) \ , \\
\rho^{(0)} &= \rho_x(1)\rho_y^A(\gamma) \ , \\
U^{(0)} &= -\frac{\partial}{\partial\beta}\ln Z^0 = U_x(1) + U_y^A(\gamma) \ , \\
S^{(0)} &= k_B\left(1-\beta\frac{\partial}{\partial\beta}\right)\ln Z^0 = S_x(1) + S_y^A(\gamma) \ .
\end{aligned}
$$

After Insertion:

$$
\begin{aligned}
Z^{(I)} &= \left(Z_x^L(\delta) + Z_x^R(1-\delta)\right) Z_y^A(\gamma) \ , \\
\rho^{(I)} &= \left(p^L(\delta)\rho_x^L(\delta) + p^R(1-\delta)\rho_x^R(1-\delta)\right) \rho_y^A(\gamma) \ , \\
U^{(I)} &= -\frac{\partial}{\partial\beta}\ln Z^I \ , \\
S^{(I)} &= k_B\left(1-\beta\frac{\partial}{\partial\beta}\right)\ln Z^I \ .
\end{aligned}
$$

Here $p^L(\delta)$ and $p^R(1-\delta)$ are the probabilities of finding the particle in the left and the right sides of the box, respectively:

$$p^L(\delta) = \frac{Z_x(\delta)}{Z_x(\delta) + Z_x(1-\delta)} \text{ and}$$
$$p^R(1-\delta) = \frac{Z_x(1-\delta)}{Z_x(\delta) + Z_x(1-\delta)} .$$

Measurement: The average change of the internal energy, heat transfer, and work after measurement are:

$$\langle \Delta U^M \rangle = -p^R(1-\delta)\frac{\partial}{\partial\beta}\left(\ln\frac{Z^B(1-\gamma)}{Z^A(\gamma)}\right) ,$$
$$\frac{\langle \Delta S^M \rangle}{k_B} = p^L(\delta)\ln p^L(\delta) + p^R(1-\delta)\ln p^R(1-\delta) + p^R(1-\delta)\left(1-\beta\frac{\partial}{\partial\beta}\right)\ln\frac{Z^B(1-\gamma)}{Z^A(\gamma)} ,$$
$$\beta\langle W^M \rangle = p^L(\delta)\ln p^L(\delta) + p^R(1-\delta)\left[\ln p^R(1-\delta) + \ln\frac{Z^B(1-\gamma)}{Z^A(\gamma)}\right] .$$

Control: The average change of the internal energy and the work extracted from the isothermal expansion are:

$$\langle \Delta U^C \rangle = -\frac{\partial}{\partial\beta}\ln\frac{Z_x(1)}{(Z_x(\delta)+Z_x(1-\delta))} \text{ and}$$
$$\beta\langle \Delta W^C \rangle = \ln Z_x(1) - p^L(\delta)\ln Z_x(\delta) - p^R(1-\delta)\ln Z_x(1-\delta) .$$

Erasure: The average change of the internal energy, entropy, and the work extracted during erasure are:

$$\langle \Delta U^E \rangle = -p^R(1-\delta)\frac{\partial}{\partial\beta}\ln\frac{Z^A(\gamma)}{Z^B(1-\gamma)} ,$$
$$\langle \Delta S^E \rangle = p^R(1-\delta)k_{\mathrm{B}}\left(1-\beta\frac{\partial}{\partial\beta}\right)\ln\frac{Z^A(\gamma)}{Z^B(1-\gamma)} ,$$
$$W^E = p^R(1-\delta)\beta\ln\frac{Z^A(\gamma)}{Z^B(1-\gamma)} .$$

[1] J. C. Maxwell. *Theory of Heat*. Longmans, Green and Co., London, United Kingdom, ninth edition, 1888. 1

[2] J. . A. Wheeler. The computer and the universe. *Intl. J. Theo. Phys.*, 21(6/7):557–572, 1982. 1

[3] J. A. Wheeler. Information, physics, quantum: The search for links. In W. Zurek, editor, *Entropy, Complexity, and the Physics of Information*, volume VIII of *SFI Studies in the Sciences of Complexity*, Reading, Massachusetts, 1990. Addison-Wesley.

[4] R. Landauer. Information is physical. *Physics Today*, pages 23–29, May 1991. 1

[5] L. Szilard. On the decrease of entropy in a thermodynamic system by the intervention of intelligent beings. *Z. Phys.*, 53:840–856, 1929. 1

[6] R. Landauer. Energy requirements in communication. *App. Phys. Lett.*, 51(24):551–562, 1987. 1

[7] C. H. Bennett. Thermodynamics of computation—A review. *Intl. J. Theo. Phys.*, 21(3-4):905, 1982. 1

[8] H. Leff and A. Rex. *Maxwell's Demon 2: Entropy, Classical and Quantum Information, Computing*. Taylor and Francis, New York, 2002. 1

[9] U. Seifert. Stochastic thermodynamics, fluctuation theorems and molecular machines. *Rep. Prog. Phys.*, 75:126001, 2012. 1

[10] J. M. R. Parrondo, J. M. Horowitz, and T. Sagawa. Thermodynamics of information. *Nature Physics*, 11:131–139, 2015. 1

[11] A. B. Boyd and J. P. Crutchfield. Maxwell demon dynamics: Deterministic chaos, the Szilard map, and the intelligence of thermodynamic systems. *Phys. Rev. Let.*, 116:190601, 2016. 1, 2, 6, 8

[12] A. B. Boyd, D. Mandal, and J. P. Crutchfield. Identifying functional thermodynamics in autonomous Maxwellian ratchets. *New J. Physics*, 18:023049, 2016. 1

[13] M. Hamed Mohammady and J. Anders. A quantum Szilard engine without heat from a thermal reservoir. *New J. Phys.*, 2017. 1, 7

[14] W. Zurek. Eliminating ensembles from equilibrium statistical physics: Maxwell's demon, Szilard's engine, and thermodynamics via entanglement. *Phys. Rep.*, 755:1–21, 2018. 4, 8

[15] R. Alicki and M. Horodecki. Information-thermodynamics link revisited. *J. Phys. A: Math. Theor.*, 2019.

[16] T. Sagawa and M. Ueda. Minimal energy cost for thermodynamic information processing: measurement and information erasure. *Phys. Rev. Let.*, 102(25):250602, 2009. 8

[17] T. Sagawa and M. Ueda. Erratum: minimal energy cost for thermodynamic information processing: measurement and information erasure [phys. rev. lett. 102, 250602 (2009)]. *Phys. Rev. Lett.*, 106(18):189901, 2011. 8

[18] H. Li, J. Zou, J.-G. Li, B. Shao, and L.-A. Wu. Revisiting the quantum Szilard engine with fully quantum considerations. *Ann. Physics*, 327(12):2955–2971, 2012. 8

[19] A. Aydin, A. Sisman, and R. Kosloff. Landauer's principle in a quantum Szilard engine without Maxwell's demon. *Entropy*, 22(3):294, 2020. 8

[20] S. W. Kim, T. Sagawa, S. De Liberato, and M. Ueda. Quantum Szilard engine. *Phys. Rev. Let.*, 106(7):070401, 2011.

[21] C. Y. Cai, H. Dong, C. P. Sun, et al. Multiparticle quantum Szilard engine with optimal cycles assisted by a Maxwell's demon. *Phys. Rev. E*, 85(3):031114, 2012.

[22] H. J. Jeon and S. W. Kim. Optimal work of the quantum Szilard engine under isothermal processes with inevitable irreversibility. *New J. Physics*, 18(4):043002, 2016.

[23] J. Bengtsson, M. N. Tengstrand, A. Wacker, P. Samuelsson, M. Ueda, H. Linke, and S. M. Reimann. Quantum Szilard engine with attractively interacting bosons. *Phys. Rev. Let.*, 120(10):100601, 2018.

[24] J. Song, S. Still, R. D. H. Rojas, I. P. Castillo, and M. Marsili. Optimal work extraction and mutual information in a generalized Szilard engine. *arXiv preprint arXiv:1910.04191*, 2019.

[25] Z. Zhuang and S.-D. Liang. Quantum Szilard engines with arbitrary spin. *Phys. Rev. E*, 90(5):052117, 2014.

[26] Y. Lu and G. L. Long. Parity effect and phase transitions in quantum Szilard engines. *Phys. Rev. E*, 85(1):011125, 2012.

[27] K.-H. Kim and S. W. Kim. Szilard's information heat engines in the deep quantum regime. *J. Korean Physical Soc.*, 61(8):1187–1193, 2012. 8

[28] J. Bengtsson, M. N. Tengstrand, and S. M. Reimann. Bosonic Szilard engine assisted by Feshbach resonances. *Phys. Rev. A*, 97(6):062128, 2018.

[29] H. Dong, D. Z. Xu, C. Y. Cai, C. P. Sun, et al. Quantum Maxwell's demon in thermodynamic cycles. *Phys. Rev. E*, 83(6):061108, 2011. 1, 7, 8

[30] J. V. Koski, V. F. Maisi, and J. P. Pekola. Experimental realization of a Szilard engine with a single electron. *Proc. Natl. Acad. Sci. USA*, 111(38):13786–13789, 2014. 1, 7, 8

[31] P. A. Camati, J. P. S. Peterson, T. B. Batalhao, K. Micadei, A. M. Souza, R. S. Sarthour, I. S. Oliveira, and R. M. Serra. Experimental rectification of entropy production by Maxwell's demon in a quantum system. *Phys. Rev. Let.*, 117(24):240502, 2016.

[32] W-B Wang, X-Y Chang, F Wang, P-Y Hou, Y-Y Huang, W-G Zhang, X-L Ouyang, X-Z Huang, Z-Y Zhang, H-Y Wang, et al. Realization of quantum Maxwell's demon with solid-state spins. *Chinese Phys. Let.*, 35(4):040301, 2018. 8

[33] J. P. S. Peterson, R. S. Sarthour, and R. Laflamme. Implementation of a quantum engine fueled by information. *arXiv:2006.10136*, 2020. 8

[34] M. D. Vidrighin, O. Dahlsten, M. Barbieri, M. S. Kim, V. Vedral, and I. A. Walmsley. Photonic Maxwell's demon. *Phys. Rev. Let.*, 116(5):050401, 2016. 8

[35] N. Cottet, S. Jezouin, L. Bretheau, P. Campagne-Ibarcq, Q. Ficheux, J. Anders, A. Auffeves, R. Azouit, P. Rouchon, and B. Huard. Observing a quantum Maxwell demon at work. *Proc. Natl. Acad. Sci.*, 114:7561, 2017. 8

[36] M. Naghiloo, J. J. Alonso, A. Romito, E. Lutz, and K. W. Murch. Information gain and loss for a quantum Maxwell's demon. *Phys. Rev. Let.*, 121:030604, 2018. 1, 7

[37] K. J. Ray and J. P. Crutchfield. Variations on a demonic theme: Szilard's other engines. *Chaos*, 30(9):0012052, 2020. 1, 8

[38] R. Landauer. Irreversibility and heat generation in the computing process. *IBM J. Res. Develop.*, 5(3):183–191, 1961. 1, 6

[39] M. A. Nielsen and I. L. Chuang. *Quantum Computation and Quantum Information*. Cambridge University Press, Cambridge, United Kingdom, tenth anniversary edition, 2011. 3

[40] Y. N. Joklegar. Particle in a box with a δ-function potential: Strong and weak coupling limits. *Am. J. Phys.*, 2009. 4

[41] P. Pedram. Exact solutions of a particle in a box with a delta function potential: The factorization method. *Am. J. Phys.*, 2010. 4

[42] K. Shizume. Heat generation required by information erasure. *Phys. Rev. E*, 52(4):3495–3499, 1995. 7

[43] F. N. Fahn. Maxwell's demon and the entropy cost of information. *Found. Physics*, 26:71–93, 1996.

[44] M. M. Barkeshli. Dissipationless information erasure and Landauer's principle. *arXiv:cond-mat: 0504323*.

[45] T. Sagawa. Thermodynamics of information processing in small systems. *Prog. Theo. Phys.*, 127(1):1–56, 2012. 7

[46] O. Shenker and M. Hemmo. Maxwell's demon in quantum mechanics. *Entropy*, 22(3):269, 2020. 7

[47] W. Zurek. Maxwell's daemon, szilard's engine and quantum measurements. *Frontiers of Nonequilibrium Statistical Physics*, NATO ASI Series B: Physics 135, G. T. Moore & M. O. Scully, eds. New York: Plenum., 1986. 8

[48] S. Lloyd. Quantum-mechanical Maxwell's demon. *Phys. Rev. A*, 56(3374), 1997. 8

[49] P. S. Pal and A. M. Jayannavar. Maxwell's demon, Szilard engine and Landauer principle. *Resonance*, page 443, 2021. 8

[50] P. Bracken. A quantum version of the classical Szilard engine. *Central Europ. J. Physics*, 12(1):1–8, 2014. 8

[51] J. Gea-Banacloche. Splitting the wave function of a particle in a box. *Am. J. Physics*, 70(3):307–312, 2002.

[52] V. B. Sørdal and J. Bergli. Quantum particle in a split box: Excitations to the ground state. *Phys. Rev. A*, 99(2):022121, 2019. 8